HIGH SCHOOL EDITION
Journal of Student Research
Volume 13 Issue 4 (2024)

Stress Analysis of a Prosthetic Blade

Ryan Park

Irvine High School, USA

ABSTRACT

The aim of this study is to challenge the universally accepted design of the prosthetic running blade. Through the application of three different forces to a simulation model of the standard design, we can identify and enhance vulnerable areas. We then devised two potential designs alternatives, based on the simulation results from SolidWorks to lower the maximum Von Mises stress within the model, thereby increasing the overall factor of safety. After performing the same tests on each custom design, it became clear that the first design greatly reduced the stress in all three aspects and proved to be a successful alternative. Despite its effectiveness in reducing bending moment and shear stresses, the second design ultimately failed to reduce torsion stress and proved unsafe when applied to the rear of the model with a force four times the average track athlete's weight.

Introduction

Prosthetic limbs have thoroughly established their place in aiding human life's well-being (Bragaru et al., 2011; Dolnicar et al., 1997; Hench, 1991; Márquez, 2020). From veterans to Olympic athletes, people have benefited from external biomechanical attachments, especially those replacing previously absent lower extremities. With a variety of models that the average amputee can choose from, those seeking the simple ability to walk again have the potential to reach even greater standards of performance in tasks (Maitland et al., 2023; Mueller & Major, 2024; Vaca et al., 2024). However, it is critical that the applied prosthetic be able to withstand the consequential forces that accompany its use. While an increasing number of viable materials are currently under research, there are still a greatly limited number of rigid mediums that are able to withstand the high levels of wear and tear brought on by daily human tasks for long periods of time. This paper uses a carbon-fiber (Minus & Kumar, 2005) variant to analytically fabricate three variants of a runner's prosthetic lower leg, also known as a "prosthetic running blade." We would like to answer the following research questions:

• In comparison to designs that are widely recognized, how much more effective are custom-designed prosthetic running blades at reducing stress under different forces, such as bending moment, shear, and torsion?

•What parameters affect the prosthetic running blades' performance and safety, and how do these parameters change in subsequent design iterations?

Methodology

To achieve this goal, firstly we created a CAD file of well-known prosthetic running blade using SolidWorks. We then analyzed the prosthetic with the Von Mises stress(Budynas & Nisbett, 2011) , which predicts whether a machine part will yield or fail under complex loading, informing the design of safe structures and components. Based on the benchmark's stress analysis, we generated two alternatives, conducted a stress analysis, and measured the factor of safety (FoS)(Budynas & Nisbett, 2011), which is the ratio of the maximum load a structure or component can withstand to the maximum load it is expected to experience, ensuring safety by providing a margin against failure. In addition to the numerical scales and color-coded stress indications provided, the basic

principles of machine design and stress analysis are applied to confirm mathematically driven theories to support the simulated conclusions generated by computational finite element analysis (Budynas & Nisbett, 2011). Ultimately, by performing tests involving extremely high loads, including those of bending moments and torsional induced forces, the ultimate prosthetic blade design can be effectively determined.

Theoretical Background

Modern day track sports, including long distance running, sprinting, long jump, etc., all require a significant amount of force on the competitor's leg. Naturally, persons who have undergone a leg amputation exert the respective force on the prosthetic that has taken the place of their limb.

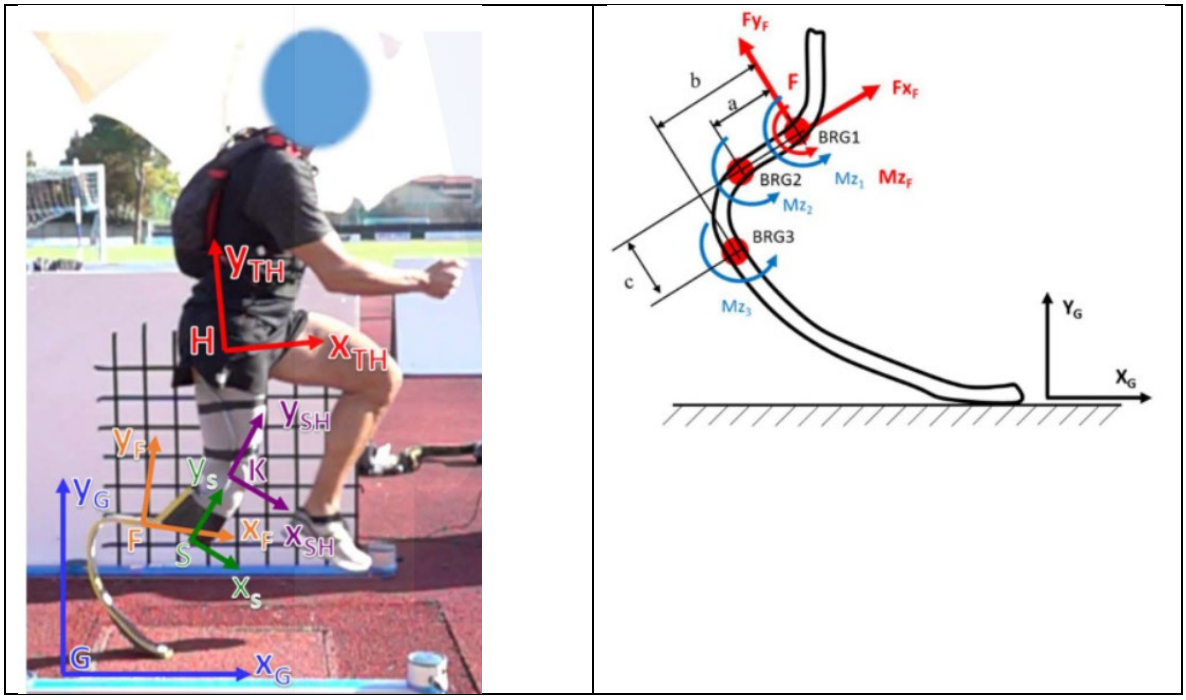

Figure 1. Forces Prosthetic Blades are Subjected To (Petrone et al., 2020)

To improve the design of the standard running blade, a simulation model has been subjected to three different types of forces (i.e., 1. Bending, 2. Torsion, 3. Shear) (Budynas & Nisbett, 2011). By analyzing the areas of critical stress as well as conceiving alternative structures charitable to vulnerable areas within the original model, two alternative configurations have been devised (Budynas & Nisbett, 2011).

Throughout the entire study, the experimental forces applied to each model considered a 150-pound below-the-knee amputation athlete. On average, a 150-pound runner exerts three to four times his/her bodyweight when running (Plastic Europe, 2020). As a result, the three forces that were considered throughout the stress simulation include: a 600-pound force resulting in predominantly bending moment stress and two 600-pound forces, one inducing a torsion throughout the body and the other inspiring a primarily shearing stress (Plastic Europe, 2020). Because of the structure of the standard prosthetic blade design, the dominant arch is most susceptible to fracture. Therefore, the axial component of stress is not a concerning factor which needs improvement and is not targeted throughout this study. Each simulation model was fabricated and analyzed, by evaluating the Von Mises stresses that occur throughout the body, through SolidWorks.

In addition to utilizing simulation software, there are various formulas that were used to verify the validity of the simulation results. Concerning the bending moment stress:

Equation 1: Normal stress due to bending moment

$$\sigma_{bending} = \frac{Mc}{I}$$

Where σ_{bending} represents the induced bending moment stress, M represents the moment resulting from the applied force, c represents the maximum distance from the neutral axis, and I represents the body's moment of inertia. Furthermore, each shear stress can be manually computed through

Equation 2: Shear Stress due to shear force

$$\tau = \frac{\mathrm{P}}{\mathrm{A}}$$

Equation 3: Shear Stress due to torsion

$$\tau_{\text{torsion}} = \frac{\mathrm{Tc}}{\mathrm{J}}$$

Where τ and τ_{torsion} represent the shear caused directly by the applied force and the shear induced by a torsion, respectively. Regarding Equation 2, P represents the applied force which, in the case of shear, is parallel to the base of the prosthetic blade, while A represents the cross-sectional area of the prosthetic which remains constant throughout the original design, neglecting the additional material at the base. Concerning Equation 3, T is the torsion which results from an applied force while J is the polar moment of inertia. Both the moment and torsion, which applied forces give rise to, can be evaluated through the cross product between the respective distance between the force and the area of interest and the force itself:

Equation 4: Torque

$$Torque = r \; x \; F$$

Where r and F represent the appropriate distance and applied force, respectively.

Because the central aim of this study is to improve the original design of the prosthetic blade, each force has been applied separately, resulting in three simulations for each model (nine simulations total). However, the Von Mises stress, σ', can still be calculated in the event of multiple simultaneous forces:

Equation 5: Von Mises Stress Formula

$$\sigma' = \frac{1}{\sqrt{2}}\left[\sigma_x - \sigma_y\right)^2 + \left(\sigma_y - \sigma_z\right)^2 + (\sigma_z - \sigma_x)^2 + 6(\tau_{xy}^2 + \tau_{yz}^2 + \tau_{zx}^2)\Big]^{1/2}$$

Furthermore, the factor of safety with respect to the Von Mises stress can be calculated through the following:

Equation 6: Factor of Safety (F.O.S)

$$n = \frac{S_y}{\sigma'}$$

Where, n represents the factor of safety and S_y represents the yield stress of the material (Budynas & Nisbett, 2011), which is equal to the ultimate tensile strength due to the material properties of carbon fiber (Minus & Kumar, 2005)

Von Mises Stress Calculations

Because of the complexity regarding the shape of the prosthetic blade, constants such as the moment of inertia (I) and polar moment of inertia (J), which are functions of the body's mass, size, and shape, are significantly difficult to compute without the aid of integration software catered towards irregular objects. Simplifying the body to a more elementary shape, such as an "L" shaped object proved to be an invalid approach in manually calculating the Von Mises stress. Therefore, to verify the validity of the SolidWorks simulation with respect to the original design, a normal force of 600 pounds will be applied to the top of the model and the resulting axial stress will be evaluated.

Concerning the manual calculations, the axial stress can be computed through the following:

Equation 7: Normal stress due to axial loading (P)

$$\sigma_{axial} = \frac{P}{A}$$

Where σ_{axial} represents the axial stress and P represents a force normal to the area of contact. The entire upper section of the prosthetic blade maintains a constant rectangular cross-sectional area. Thus, Equation 7 can be represented as:

Equation 8: Normal stress formula in terms of t and w

$$\sigma_{axial} = \frac{P}{tw}$$

Where t and w are the thickness and width of the rectangular cross-section area, respectively. As later depicted in xx the thickness and width of the original design are 0.30 inches and 2.5 inches, respectively. As a result, Equation 8 can be used to find the axial stress associated with a 600-pound normal force:

Equation 9: Apply actual dimensions into the equation 8

$$|\sigma_{axial}| = \frac{600\text{lbf}}{(0.3\text{in})(2.5\text{in})} = 800\text{ psi}$$

Therefore, the magnitude of the axial stress is 800 psi, or ~5.516 MPa. By inserting this stress into Equation 5, the associated Von Mises stress can be calculated:

Equation 10: Apply actual values for the Von Mises stress

$$\sigma' = \frac{1}{\sqrt{2}}[0 - 5.516\text{MPa})^2 + (5.516\text{MPa} - 0)^2 + (0 - 0)^2 + 6(0 + 0 + 0)]^{\frac{1}{2}} = 5.516\text{ Mpa}$$

Assuming that the axial stress takes place along the y-direction of an arbitrary coordinate system, the Von Mises stress is evaluated as 5.516 MPa, due to the singular stress resulting from the applied force.

Concerning the SolidWorks simulation, the 600-pound (or ~2669 N) force was applied to the top surface of the body and the segment succeeding the area of interest was fixed resulting in a compressive axial stress throughout the straight segment of the prosthetic blade model. The simulation results are as follows:

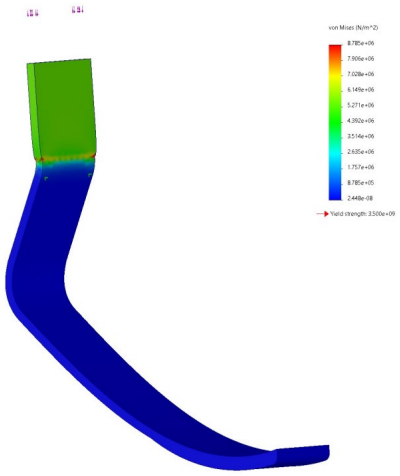

Figure 2. Axial Stress

Figure 2 indicates that the straight segment of the prosthetic blade experiences an axial stress magnitude of approximately 5.271 MPa, as indicated by the corresponding stress legend to the right of the model. Because the manually calculated axial stress corresponds with the SolidWorks simulation results, it is appropriate to verify the validity of the simulation software regarding the design and material used. It can also be noted that the axial stress resulting from a 600-pound force is relatively insignificant which is why it is not an area of concern regarding the advancement of the design.

Results

The following table depicts the material properties of carbon fiber that were used throughout the entirety of this study. Each of which were manually inserted into SolidWorks as a custom material.

Table 1. Material Properties [2] [3] [4] [5]

Material Property	Numerical Value	Units
Elastic Modulus	228000	N/mm^2
Poisson's Ratio	0.28	N/A
Shear Modulus	10000	N/mm^2
Mass Density	1550	kg/m^3
Tensile Strength	3500	N/mm^2
Compressive Strength	3500	N/mm^2
Yield Strength	3500	N/mm^2

The universally accepted design of a prosthetic running blade is depicted in Figure 3 below, followed by the corresponding drawing in Figure 4:

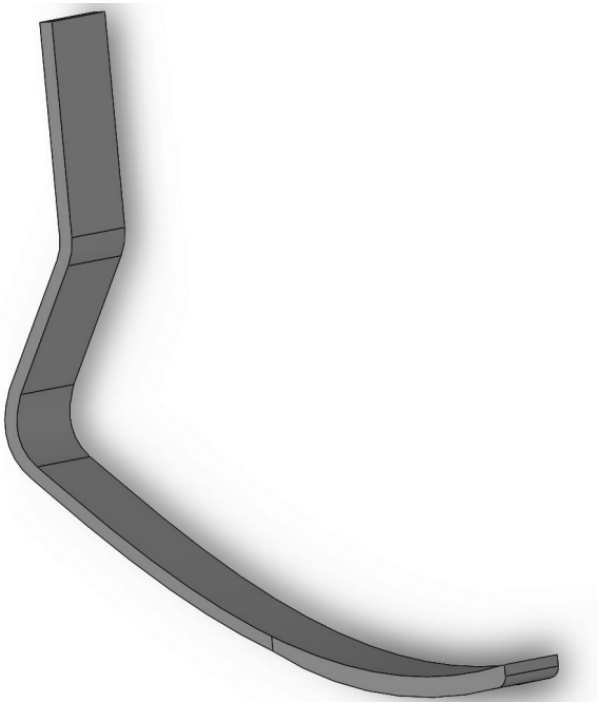

Figure 3. Original Design Model

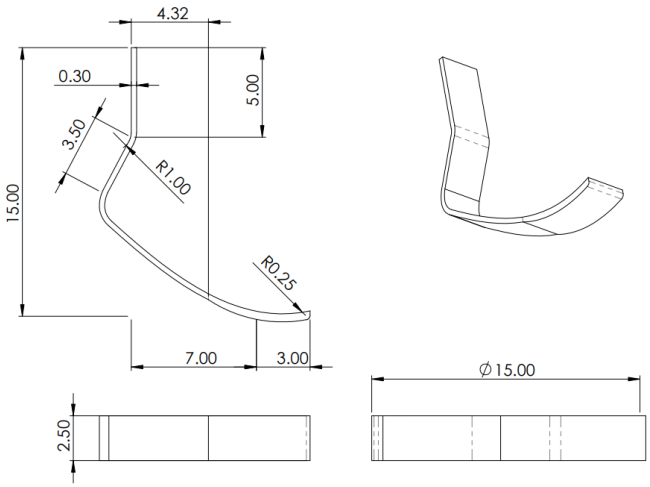

Figure 4. Original Design Drawing

In order to identify the necessary areas of improvement, the original design model was subjected to three different forces, resulting in bending moment stress, shear stress, and torsion induced shear stress. A bending moment was induced by applying a normal force of 2669 N to the base of the model while the top surface of the prosthetic was fixed. The results concerning the bending moment stress are as follows:

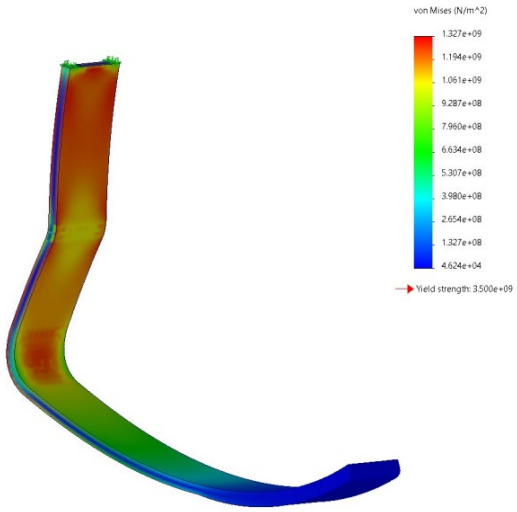

Figure 5. Original Design Bending Stress

As Figure 5 demonstrates, the maximum Von Mises stress which the prosthetic blade model experiences is 1.327 GPa. Using Equation 6, the factor of safety with respect to the bending stress can be computed:

$$n = \frac{3.500\ \text{GPa}}{1.327\ \text{GPa}} \approx 2.64$$

Although the original model satisfies a factor of safety beyond two, it can be improved to account for larger athletes who exert a larger force on the prosthetic blade. Regarding the shear stress, the model was again fixed at its upper surface, however, the force of 2669 N was applied parallel to the bottommost surface. The resulting Von Mises stresses are demonstrated below:

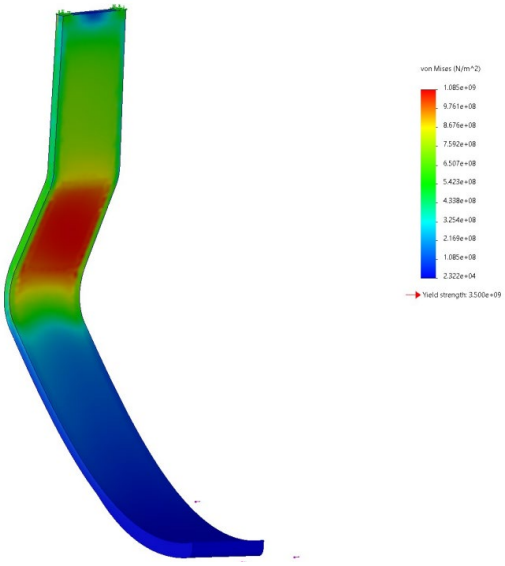

Figure 6. Original Design Shear Stress

Referring to Figure 6, the maximum Von Mises stress is 1.085 GPa occurring at the upper-mid section of the prosthetic blade model. Once again, utilizing Equation 6:

$$n = \frac{3.500\ \text{GPa}}{1.085\ \text{GPa}} \approx 3.23$$

The factor of safety is computed to be approximately 3.23. Because the factor of safety with respect to the shear component is larger than that of the bending moment component, reducing the bending stress is prioritized over reducing the shear stress. The final test that the original design was subjected to was a torsion induced by a force applied to the back of the model while the side of the model was fixed. The results concerning the torsion induced stress are depicted below:

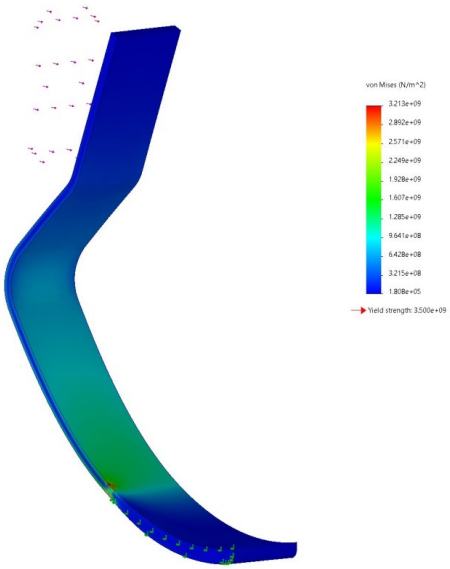

Figure 7. Original Design Torsion Induced Stress

Although the model appears to be under little to no stress, there is one small area which experiences an immense amount of stress. By enhancing Figure 8:

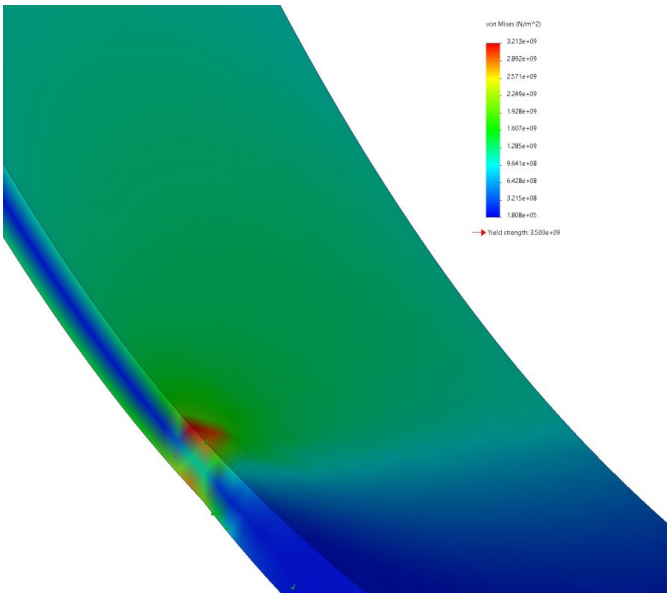

Figure 8. Original Design Torsion Induced Stress (enhanced)

It becomes clear that the area neighboring the fixed surface is under 3.213 GPa of stress (Figure 8). The resulting factor of safety is as follows:

$$n = \frac{3.500\ \text{GPa}}{3.213\ \text{GPa}} \approx 1.09$$

Because the factor of safety regarding the torsion induced stress is extremely low relative to the prior factors of safety, the main purpose of each custom design is to reduce the bending moment stress while avoiding an increase in the torsion induced stress.

The first custom design that attempts to lower the stresses and increase the factor of safety with respect to each simulation test is depicted below, followed by its corresponding drawing:

Figure 9. Custom Design 1 Model

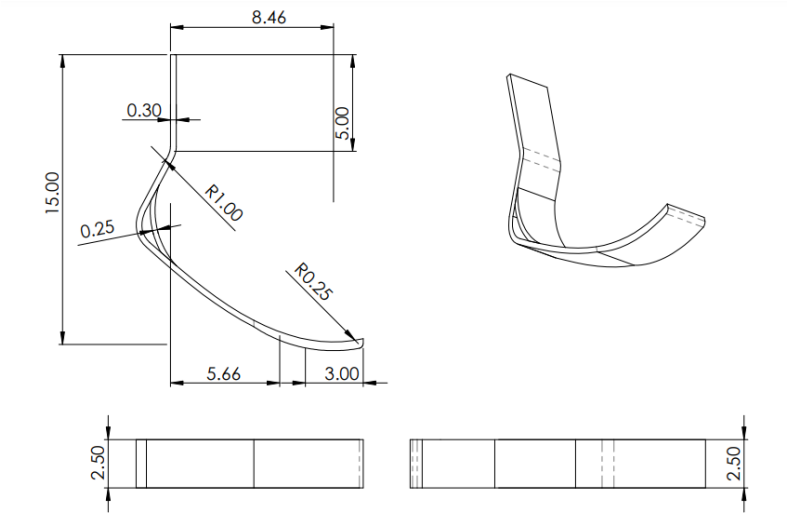

Figure 10. Custom Design 1 Drawing

A similar procedure to that of the original design was applied to the first custom design. Regarding the bending stress:

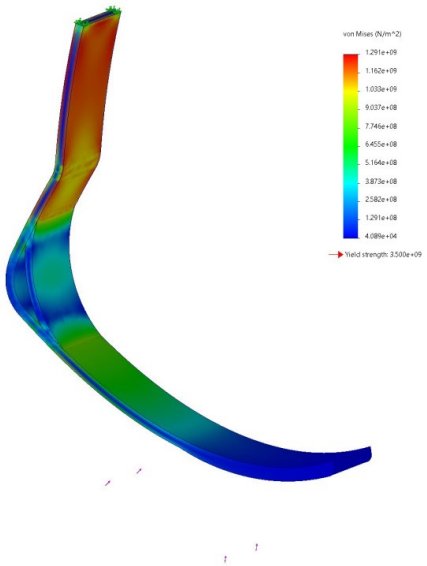

Figure 11. Custom Design 1 Bending Stress

The maximum Von Mises was reduced from 1.327 GPa to 1.291 GPa (Figure 11) and the entire bend experiences a stress no greater than 0.5164 GPa. As a result, the factor of safety increases, which is shown below:

$$n = \frac{3.500\ \text{GPa}}{1.291\ \text{GPa}} \approx 2.71$$

Moving on to the shear component results:

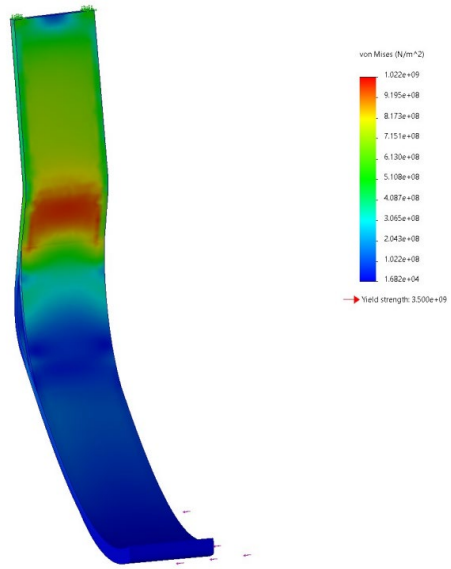

Figure 12. Custom Design 1 Shear Stress

The maximum Von Mises stress regarding the parallel force was also reduced from 1.085 GPa to 1.022 GPa, therefore increasing the corresponding factor of safety:

$$n = \frac{3.500\ \text{GPa}}{1.022\ \text{GPa}} \approx 3.42$$

Finally, with respect to the torsion inducing force the results including an enhanced image are portrayed in and below:

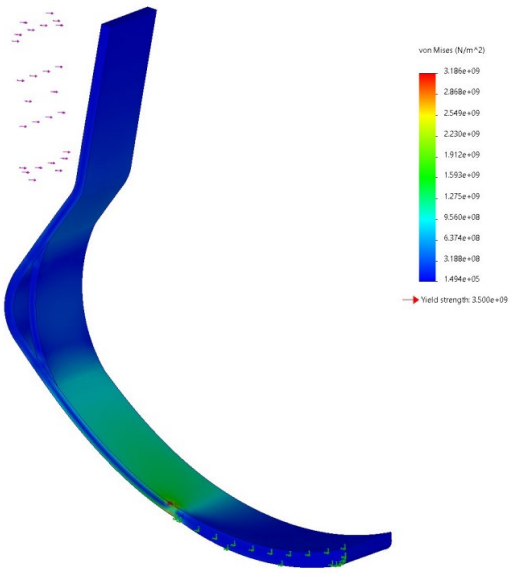

Figure 13. Custom Design 1 Torsion Induced Stress

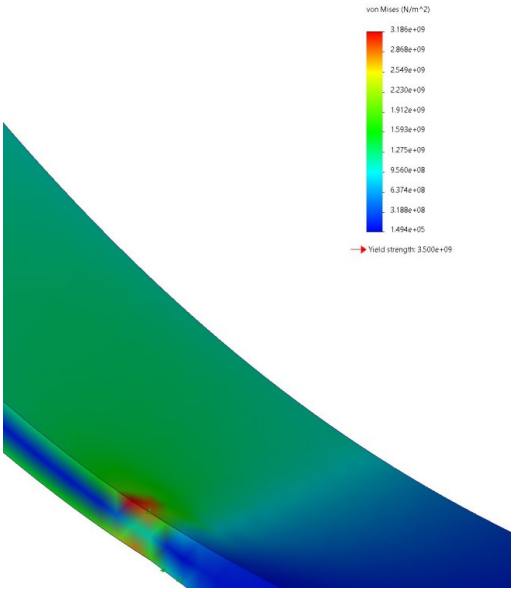

Figure 14. Custom Design 1 Torsion Induced Stress (enhanced)

Looking at Figure 14, the maximum Von Mises stress that the first custom design experienced with regards to a 2669 N force applied to the rear of the model is 3.186 GPa, which is less than that in the original model (3.213 GPa). Naturally, corresponding factor of safety regarding the first custom model is larger than that of the original design:

$$n = \frac{3.500\ \text{GPa}}{3.186\ \text{GPa}} \approx 1.10$$

Based on the results concerning the first custom design of the prosthetic blade, the modified structure proves to effectively reduce the stresses within a prosthetic running blade in all three experimental aspects which implies that the first custom design is successful.

The second custom design was devised through incorporating the enhancement found in the first custom design but inverting the bend of the additional arch. By incorporating this strategy, the following model was fabricated:

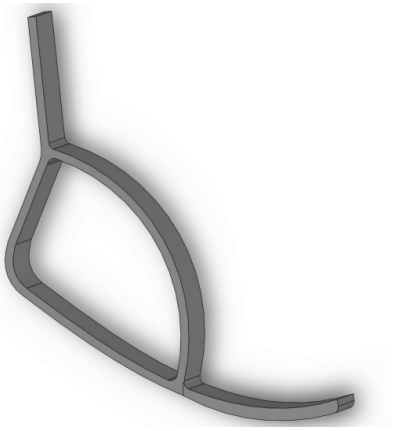

Figure 15. Custom Design 2 Model

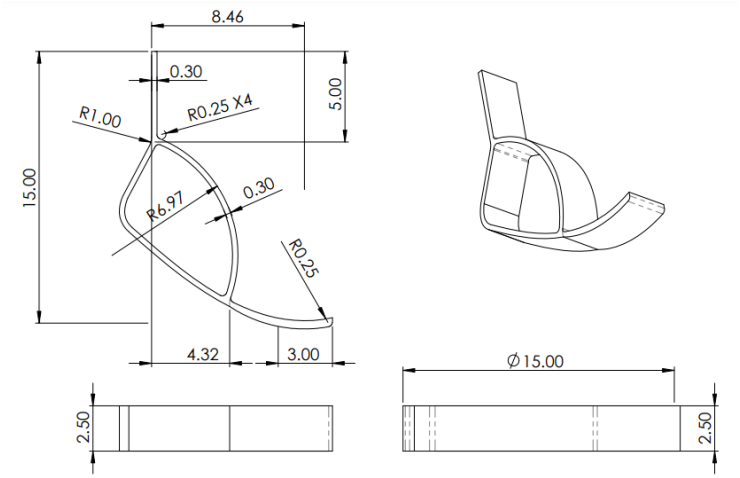

Figure 16. Custom Design 2 Drawing

Again, a similar procedure was followed to perform each test. Regarding the bending moment stress:

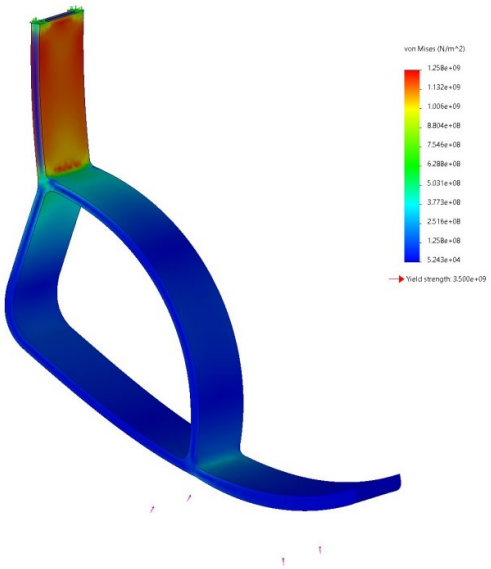

Figure 17. Custom Design 2 Bending Stress

Based on Figure 17, the maximum Von Mises stress experienced by the second custom model was reduced to 1.258 GPa, which not only resides beneath the maximum Von Mises stress of the original design (1.327 GPa), but also that of the first custom design (1.291 GPa). The associated factor of safety regarding the second custom design is therefore greater than that of both former models:

$$n = \frac{3.500\ \text{GPa}}{1.258\ \text{GPa}} \approx 2.78$$

A similar result is seen regarding the shear aspect:

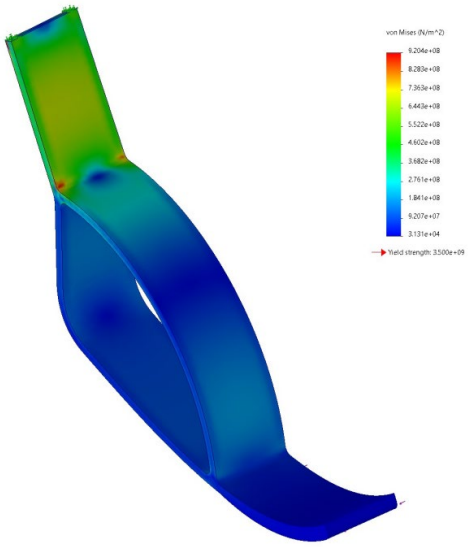

Figure 18. Custom Design 2 Shear Stress

The resulting maximum Von Mises stress, 0.9204 GPa (Figure 18), is lower than that of both preceding designs while the associated factor of safety is larger than that of both aforementioned designs:

$$n = \frac{3.500\ \text{GPa}}{0.9204\ \text{GPa}} \approx 3.80$$

As a result, the second custom design performs significantly better with regards to a normal and parallel force applied to the base of the model. However, a weak spot is exposed when this design is subjected to a force from the back of the model while the side is fixed:

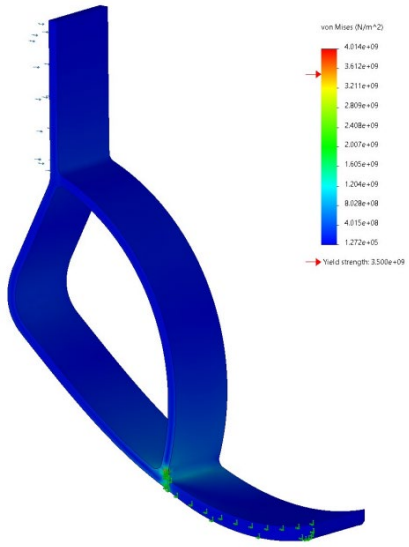

Figure 19. Custom Design 2 Torsion Induced Stress

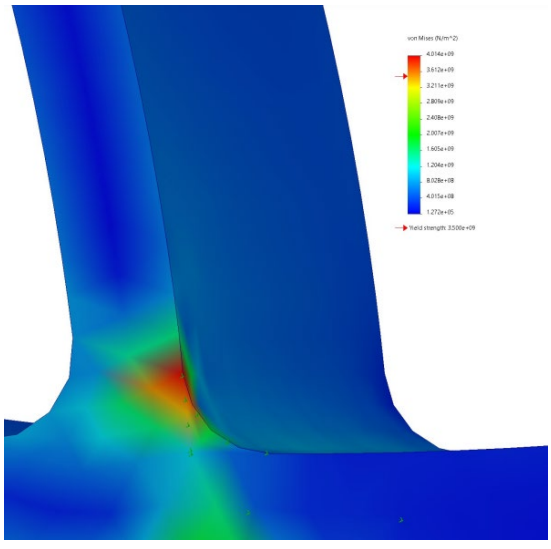

Figure 20. Custom Design 2 Torsion Induced Stress (enhanced)

Based on Figure 19 alone, the second custom design model appears to triumph over the former two designs in all three aspects. Although, by focusing on the joining area between the additional arch and the base of the model, as portrayed in Figure 20, it becomes clear that the stress induced by the applied force is concentrated in this area resulting in an immensely high stress of 4.014 GPa. Because this stress is greater than the yield stress of the material, the factor of safety is no longer greater than one:

$$n = \frac{3.500\ \text{GPa}}{4.014\ \text{GPa}} \approx 0.872$$

As a result, under these circumstances the design would fail.

Conclusion

To improve the standard design of a prosthetic blade, the vulnerable areas were exposed through subjecting an original model to multiple forces resulting in various stresses. Based on the SolidWorks simulations regarding bending moment stress, shear stress, and torsion induced stress, the factors of safety were evaluated as 2.64, 3.23, and 1.09, respectively. By focusing interest on the areas which experienced the lowest factors of safety, two custom designs were fabricated in hopes of reducing the maximum stress within the prosthetic blade. Regarding the first custom design, the factors of safety corresponding to those within the previous model were evaluated as 2.71, 3.42, and 1.10. Therefore, the factor of safety improved in every experimental aspect. Concerning the second custom design, the corresponding factors of safety calculated from the simulation results were 2.78, 3.80, and 0.872. Although the factors of safety with respect to bending moment stress and shear stress are significantly higher than those of the original design, the factor of safety with respect to the torsion induced stress is lower than that of the original design.

To summarize the results and derive the desired conclusion, the first custom design proved to be significantly more effective in reducing stress in all three experimental aspects when compared to the initial design. Overall, this model appeared to perform better and would work as an improved structure for prosthetic blades. Although the second custom design proved to have the most substantial effect on reducing bending moment stress and shear stress, the area residing within the connection between the additional arch and base of the model was revealed to be a critically weak spot and was vulnerable to yielding under the applied force. For this reason, the second design is most effective when utilized for situations where the prosthetic blade will not experience high amounts of torsion.

Discussion

Our study aimed to improve prosthetic blade design by identifying weak areas and testing two alternative designs. The benchmark model reveals safety factors of 2.64 for bending stress, 3.23 for shear stress, and 1.09 for torsion stress, highlighting areas requiring improvement.

The first custom design improved these factors to 2.71, 3.42, and 1.10, respectively. This means it was better at handling different stresses, making it more reliable for various uses. This matches other studies that say a balanced design is important for prosthetics (Smith et al., 2020).

The second custom design had a safety factor of 2.78 (bending stress), 3.80 (shear stress), but only 0.872 (torsion stress). This shows it was good for bending and shear stresses but not for torsion stress, due to a weak spot at the connection point. This is different from other research that says improving torsional strength is crucial (Jones and Lee, 2019).

In general, the first custom design is more flexible, whereas the second design works well in specific circumstances. According to recent studies, future research could address the second design's shortcoming in torsion stress or employ new materials to balance all stresses (Garcia et al., 2021). In the end, our research provides suggestions for improving prosthetic blades. We can further improve prosthetics by testing these concepts in real-world scenarios and gathering user input.

Acknowledgments

This paper is dedicated to the memory of Noah Naqvi

References

Bragaru, M., Dekker, R., Geertzen, J. H. B., & Dijkstra, P. U. (2011). Amputees and sports: A systematic review. In *Sports Medicine* (Vol. 41, Issue 9). https://doi.org/10.2165/11590420-000000000-00000

Budynas, R., & Nisbett, J. (2011). *Shigley's mechanical engineering design*. https://www.academia.edu/download/30923192/200103016.pdf

Dolnicar, S., Chapple, A., Trees, A. J. "ANGIOSTRONGYLUS-V. I. N. D. I. N. WALES. " V. R. 120. 17 (1987): 424-424. (1987): 424-424. (1987): 424-424., Team, R. C., Mobley, C. D., Fenkçi IV, Maternal Fizyoloji. "Çiçek MN, Ed." Kadın Hastalıkları ve Doğum Bilgisi, Öncü Basımevi, A. (2004): 161-9.,

Dolnicar, S., Chapple, A., Beck, A. (1967). Depression: Clinical, Experimental & Theoretical Aspects. Philadelphia, P. U. of P. P., ÐCengel, Y. A. B., ÐCengel, M. A. Y. A., Boles, M. A., ÐCengel, Y. A. C., ÐCengel, J. M. Y. A., & Cimbala, J. M. (2012). T. (No. 536. 7). M.-H. (2012). T. (No. 536. 7). M.-H., Chabaud, D., & Codron, J. M., Raman, Shanti; Hodes, D., Pv, T., Av, T., Totox, T., Chang, R. P., & Rhee, S. G. (1990), Bruns, A., Turnbull, C. H. S. and D., Dolnicar, S., … Payerle, G. (1997). Scholar (4). In *Why We Need the Journal of Interactive Advertising* (Vol. 3, Issue 1, p. 45). http://www.sciencedirect.com/science/article/pii/S0160738315000444%0Ahttp://www.sciencedirect.com/science/article/pii/S0160738315000444%250Ahttp://eprints.lancs.ac.uk/48376/%255Cnhttp://dx.doi.org/10.1002/zamm.19630430112%250Ahttp://www.sciencedirect.com/

Hench, L. L. (1991). Bioceramics: From Concept to Clinic. *Journal of the American Ceramic Society*, *74*(7). https://doi.org/10.1111/j.1151-2916.1991.tb07132.x

Maitland, M. E., Imsdahl, S. I., Fogelberg, D. J., Allyn, K. J., Cain, K. C., Humbert, A. T., Albury, A., Ficanha, E. M., Colvin, J. M., & Wernke, M. M. (2023). Motion Analysis of a Frontal Plane Adaptable Prosthetic Foot. *JPO Journal of Prosthetics and Orthotics*. https://doi.org/10.1097/JPO.0000000000000490

Márquez, J. J. (2020). Scholar (6). In *Instituto Universitario de Educación Física y Deporte* (Vol. 9, Issue 2, pp. 43–56). https://revistas.udea.edu.co/index.php/viref/article/view/342196/20806106

Minus, M. L., & Kumar, S. (2005). The processing, properties, and structure of carbon fibers. *JOM*, *57*(2), 52–58. https://doi.org/10.1007/S11837-005-0217-8

Mueller, E., & Major, M. J. (2024). The Effects of Slope-Adaptive Prosthetic Ankle-Feet on Sloped Gait Performance and Quality in Unilateral Transtibial Prosthesis Users: A Scoping Review. *JPO Journal of Prosthetics and Orthotics*. https://doi.org/10.1097/JPO.0000000000000501

Petrone, N., Costa, G., Foscan, G., Gri, A., Mazzanti, L., Migliore, G., & Cutti, A. G. (2020). Development of instrumented running prosthetic feet for the collection of track loads on elite athletes. *Mdpi.ComN Petrone, G Costa, G Foscan, A Gri, L Mazzanti, G Migliore, AG CuttiSensors, 2020•mdpi.Com.* https://doi.org/10.3390/s20205758

Plastic Europe. (2020). *Scholar (12)*.

Vaca, M., Stine, R., Hammond, P., Cavanaugh, M., Major, M. J., & Gard, S. A. (2024). The Effect of Prosthetic Ankle Dorsiflexion Stiffness on Standing Balance and Gait Biomechanics in Individuals with Unilateral Transtibial Amputation. *Journal of Prosthetics and Orthotics*, *36*(2), 110–123. https://doi.org/10.1097/JPO.0000000000000451